Supporting Information

$[A_3X][Ga_3PS_8]$ (A = K, Rb; X = Cl, Br): Promising IR Nonlinear Optical Materials Exhibiting Concurrently Strong Second-Harmonic Generation and High Laser Induced Damage Thresholds

Bin-Wen Liu, Hui-Yi Zeng, Xiao-Ming Jiang, Guan-E Wang, Shu-Fang Li, Li Xu* and Guo-Cong Guo*

Supplementary Index

1. EXPERIMENTAL SECTION

Syntheses. All starting reactants were handled inside an Ar-filled glovebox with controlled oxygen and moisture levels below 0.1 ppm. Ga metal (99.9%), P powder (99.99%), S powder (99.99%), KCl powder (99.9%), KBr powder (99.9%), RbCl powder (99.9%), RbBr powder (99.9%) and Ba metal (99.9%) were used as received without further purification. For the synthesis of target compounds, a stoichiometric mixture with an overall weight 300 mg of the starting materials Ba, Ga, P, S and AX (AX = KCl, RbCl, KBr and RbBr for **1**-**4**, respectively) as flux in a molar ratio of 1:3:1:10 were loaded into quartz tubes and then flame-sealed under vacuum (~10^{-4} Torr). The tubes were then placed into a temperature controlled muffle furnace, held at 300 °C for 5 h, subsequently heated to 780 °C over 5 h, dwelled for 4 days, and finally slowly cooled down to 350 °C before switching off the furnace power. Colorless single-crystals of the title compounds were harvested after washing with distilled water, with high-yield of 90%, 90%, 95% and 60% based on Ga for **1**-**4**, respectively. They were stable in air for several months at room temperature. It is noted that barium may play reaction promoter role in the formation of title compounds.

Single Crystal X-ray Diffraction. The single crystal diffraction data were performed on a Rigaku Pilatus CCD diffractometer equipped with a graphite-monochromated Mo Kα radiation (λ = 0.71073 Å) at 293 K. The intensity data sets were collected using a ω-scan technique and reduced using the CrystalClear software.[1] The structures were solved by direct methods and refined by full-matrix least-squares methods on F^2 with anisotropic thermal parameters for all atoms. All the calculations were performed with the Siemens SHELXTL version 5 package of crystallographic software.[2] The space groups were determined to be $Pmn2_1$ and Pm for Cl and Br-analogues, respectively, based on the intensity distribution and systematic extinction of the observed structure factors. The final structures were examined for additional symmetry with ADDSYM/PLATON.[3] The program STRUCTURE TIDY [4] was used to put the positional parameters in a standard setting. The formulas take collectively into account crystallographically refined compositions, requirements of charge neutrality. Additional crystallographic details are given in Table S1, the selected bond distances and

bond angles are given in Tables S2 and S3. Further details on the crystal structures investigation may be obtained from the Fachinformationszentrum Karlsruhe, 76344 Eggenstein-Leo-poldshafen, Germany (fax: (+49)7247-808-666; e-mail: crysda-ta@fiz-karlsruhe.de), on quoting the depository number CSD-429893 for **1**, CSD-429894 for **2**, CSD-429895 for **3**, CSD-429896 for **4**.

Powder X-ray Diffraction. Powder X-ray diffraction (XRD) data of **1-4** were obtained on an automated Rigaku MiniFlex II X-ray diffractometer equipped with a diffracted monochromator set for Cu Kα radiation (λ = 1.54057 Å), operating at 30 kV and 40 mA. The observed powder patterns were found to match well with the simulated ones based on the single-crystal structure refinements of **1-4**, respectively (Fig. S1).

Energy-Dispersive X-ray Spectroscopy (EDS) Analysis and Inductively Coupled Plasma (ICP) Measurements. Semi-quantitative EDX were performed with an EDX-equipped Hitachi S-3500 SEM spectrometer on the crystals that were used for X-ray single-crystal diffraction. The analyses of those crystals confirmed the presence each component (Fig. S2). Meanwhile, ICP had been investigated on Ultima 2 inductively coupled plasma OES spectrometer (Table S4). Both the EDS and ICP results are in according with the formula based on single-crystal refinement results.

Infrared and UV−Vis−NIR Diffuse Reflectance Spectroscopy. The optical diffuse reflectance spectra of powder samples **1-4** were measured at room temperature using a Perkin-Elmer Lambda 950 UV/Vis/NIR spectrophotometer equipped with an integrating sphere attachment in the wavelength range of 200–2500 nm and $BaSO_4$ as the reference. The absorption spectra were calculated from the reflection spectra using the Kubelka-Munk formula: $\alpha/S = (1-R)^2/2R$,[5] in which α is the absorption coefficient, S is the scattering coefficient, and R is the reflectance. IR spectra were recorded by using a Nicolet Magana 750 FT−IR spectrophotometer in the range 4000−400 cm^{-1}. Powdery samples were diluted with dry KBr and pressed into pellets before measurements.

Thermal Analysis. The thermal properties of title compounds were investigated by differential scanning calorimetric (DSC) analysis using the TGA/DSC1 Mettler Toledo

thermal analyzer (the DSC was calibrated with Al_2O_3). Polycrystalline samples (25, 32, 23 and 34 mg for **1**-**4**, respectively) were placed in sealed silica tubes evacuated to ~10^{-4} Torr and then undergo a heating/cooling cycle at a rate of 10 ℃/min. The melted residues were examined and analyzed by powder X-ray diffraction after the experiments.

Second-Harmonic Generation (SHG) Measurements. The powder SHG of **1**-**4** were estimated on microcrystalline sample by the incident 1064 nm and 1950 nm laser, using a modified Kurtz-Perry powder technique. Polycrystalline samples were ground and sieved into several distinct particle size ranges (30−50, 50−75, 75−100, 100−125, 125−150, 150−200, and 200−250 μm) for the SHG phase-matching measurements. The crystalline samples of AGS with same particle size ranges were served as the standard. In order to evaluate of NLO effects of the polycrystalline sample with a preferred orientation, a modified rotary sample stage for SHG tests were prepared (that is, a quartz tube with the diameter of 1.8 mm that can be filled with powdery sample was perpendicularly inserted into a rotary stage that can be rotated precisely from 0 to 360^o)，the powdery samples were put into the round quartz tubes, and the top and bottom of the sample were stopped by cotton fiber. The tube was rotated and the SHG intensity values of sample were recorded for each increasing 30 ^{o}. The frequency-doubling signals were detected by an Andor's DU420A-BR-DD CCD.

Laser Induced Damage Threshold (LIDT) Measurements. The powder LIDT of **1**-**4** were evaluated on microcrystalline sample (50−75 μm), with the focused high-power 1064 nm laser beam with a pulse width τ_p of 10 ns and a repetition rate of 1 Hz, using the single pulse powder LIDT measurement method. A microcrystalline AGS of same particle size range was used as a reference. The power of the laser beam was measured by a Nova II sensor display with a PE50-DIF-C energy sensor. An optical concave lens was used to adjust the diameter of the laser beam to obtain different intensities. The measurements were carried out by gradually increasing the laser power until the damage spot of samples was monitored under a magnifier after the irradiation. The damage thresholds were derived from the equation $I_{(threshold)} = E/(\pi r^2 \tau_p)$, in which E is the laser energy of a single pulse, r is the spot radius and τ_p is pulse width.

Computation Procedure. Calculations of electronic band structures were performed for **1**-**4** based on the structures and optical properties determined by single-crystal X-ray diffraction analysis. The calculation was performed with the CASTEP code [6] based on density functional theory using a plane-wave expansion of the wave functions. The total energy was calculated within the framework of a nonlocal gradient-corrected approximation, the Perdew−Burke−Ernzerhof (PBE) functional.[7] The interactions between the ionic cores and electrons are described by the norm-conserving pseudopotential.[8] The orbital electrons of K $3s^2 3p^6 4s^1$, Rb $4s^2 4p^6 5s^1$, Ga $3d^{10} 4s^2 4p^1$, P $3s^2 3p^3$, S $3s^2 3p^4$, Cl $3s^2 3p^5$ and Br $3d^{10} 4s^2 4p^5$ were treated as valence electrons, and a cutoff energy of 800 eV were set for all compounds. Monkhorst-Pack grids for Brillouin-zone *k*-point sampling used in the calculations were 3×4×1 for **1**-**2** and 4×3×3 for **3**-**4**, respectively. The calculated electronic band structures of **1**-**4** along high symmetry points of the first Brillouin zone show that the Cl-analogues are indirect band structures with the band gaps of 2.26 and 2.36 eV for **1** and **2**, whereas the Br-analogues are direct band structures with the band gaps of 2.60 and 2.48 eV for **3** and **4**, respectively (Fig. S10). Note that these band gaps are smaller than the corresponding experimental values (3.60, 3.65, 3.85, and 3.50 eV for **1**-**4**, respectively) derived from the UV−Vis diffuse reflection spectra, due to the limitation of the DFT method that sometimes underestimates the band gap for semiconductors and insulators.[9] So, scissors operators of 1.34, 1.29, 1.25 and 1.02 eV are obtained for calculations of the optical properties of **1**-**4**, respectively. The complex dielectric function $\varepsilon(\omega) = \varepsilon_1(\omega)+i\varepsilon_2(\omega)$ was calculated, of which the imaginary part $\varepsilon_2(\omega)$ generated other optical constants via the Kramers–Kroning transform.[10] The second-order susceptibilities are expressed in terms of the first-order susceptibilities as $\chi^{(2)}_{ijk}(\omega_3,\omega_1,\omega_2) = \frac{ma}{N^2 e^3}\chi^{(1)}_{ii}(\omega_3)\chi^{(1)}_{jj}(\omega_1)\chi^{(1)}_{kk}(\omega_2)$, which are derived from a classical anharmonic oscillator (AHO) model.[11] The *m*, *e* and *N* are the electron mass, electron charge and number density of atoms, respectively, and the parameter *a* characterizing the nonlinearity of the response.

2. Figures and Tables

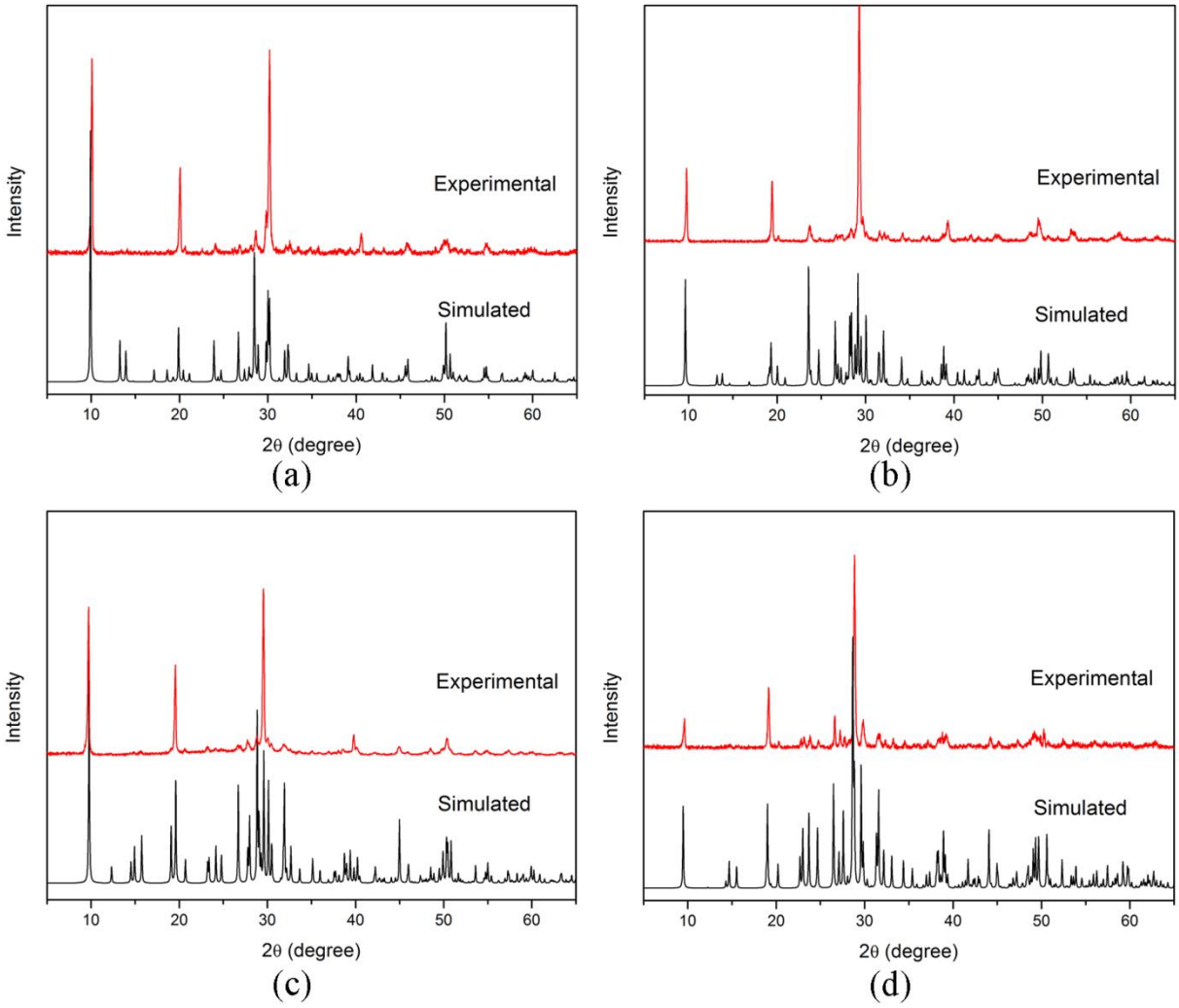

Fig. S1 Experimental (top) and simulated (bottom) powder X-ray diffraction (XRD) data of **1** (a), **2** (b), **3** (c) and **4** (d).

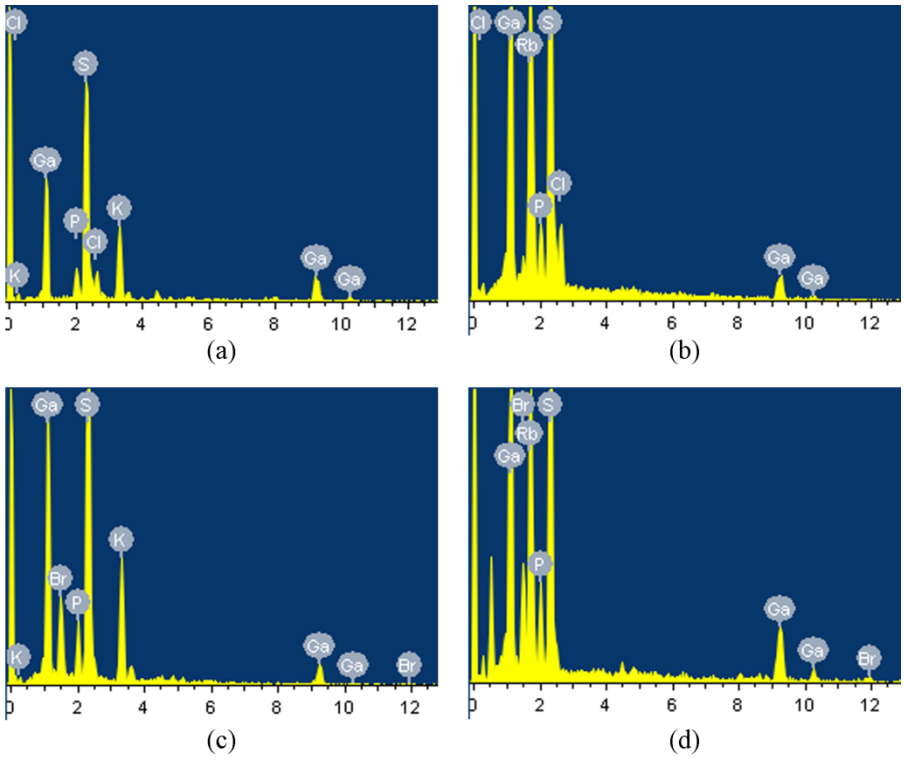

Fig. S2 EDX spectrums of **1** (a), **2** (b), **3** (c) and **4** (d).

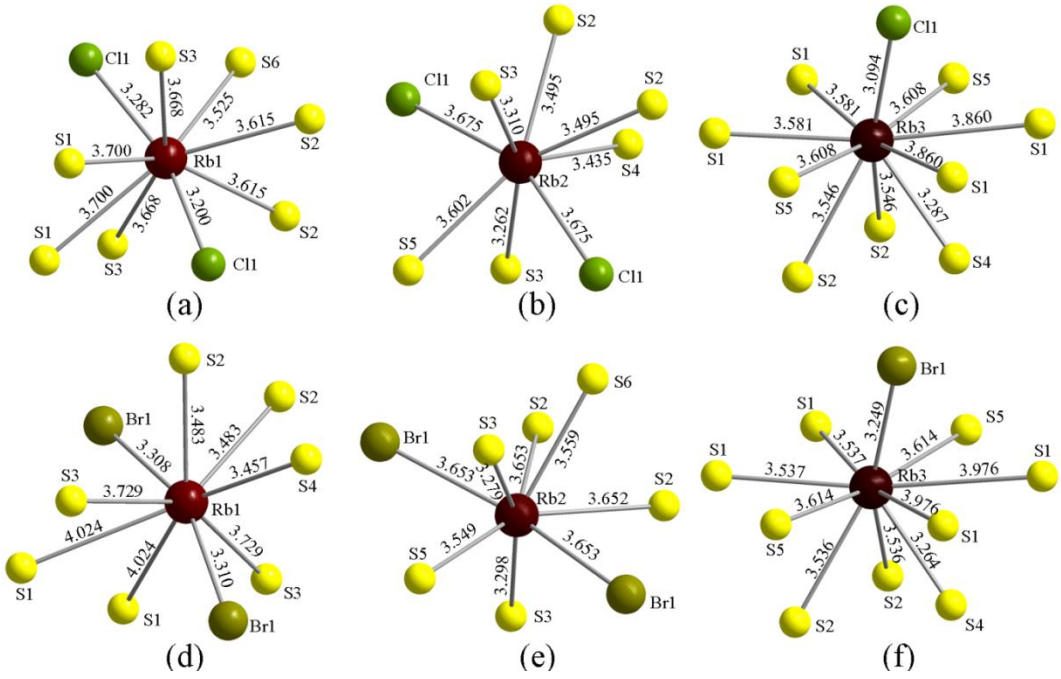

Fig. S3 Local coordination circumstance around Rb1 (a), Rb2 (b) and Rb3 (c) atom in **2**, Rb1 (d), Rb2 (e) and Rb3 (f) atoms in **4**. The atom distances (Å) are marked.

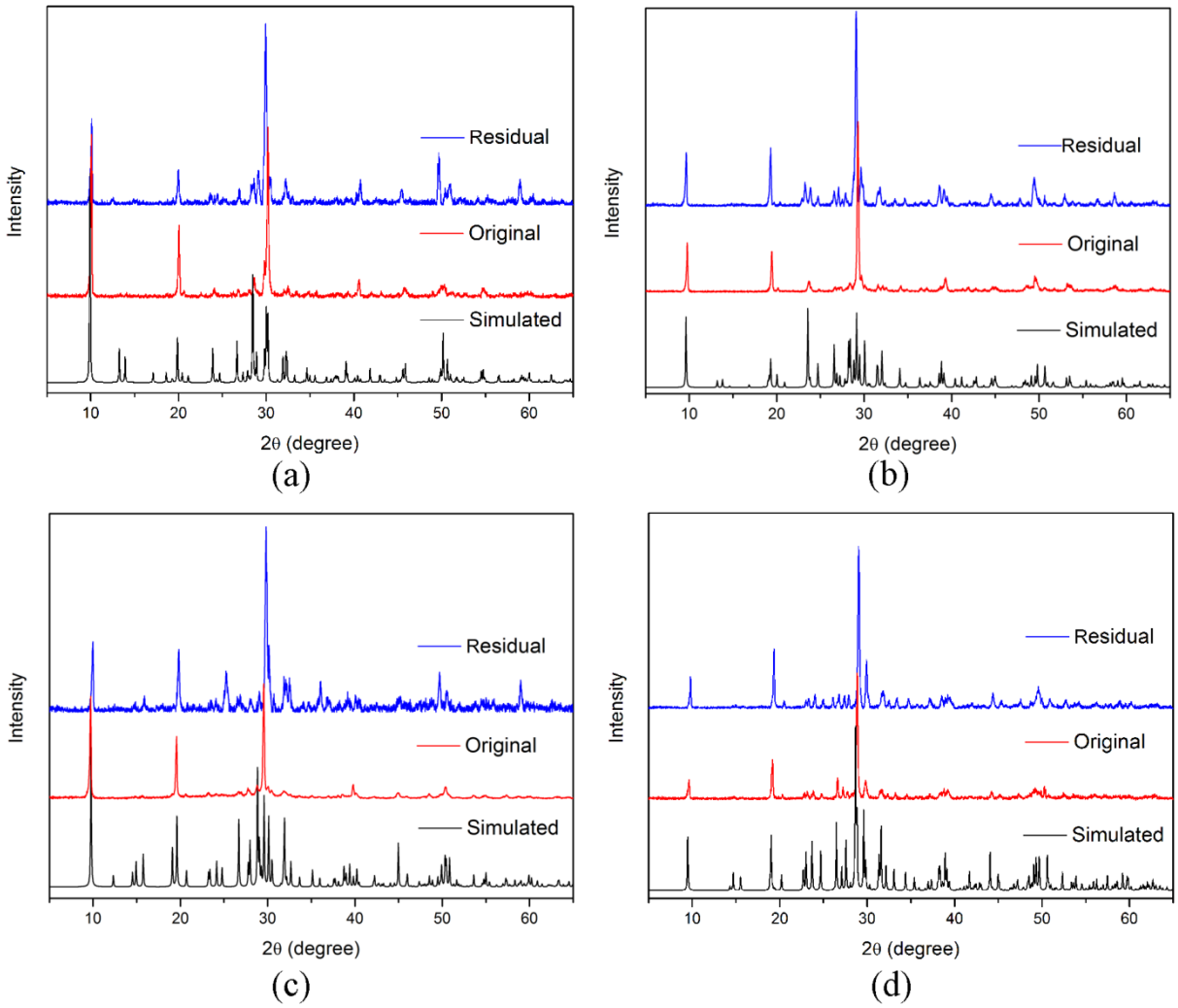

Fig. S4 X-ray powder diffraction patterns of the pristine material and the sample obtained after DTA of **1** (a), **2** (b), **3** (c) and **4** (d).

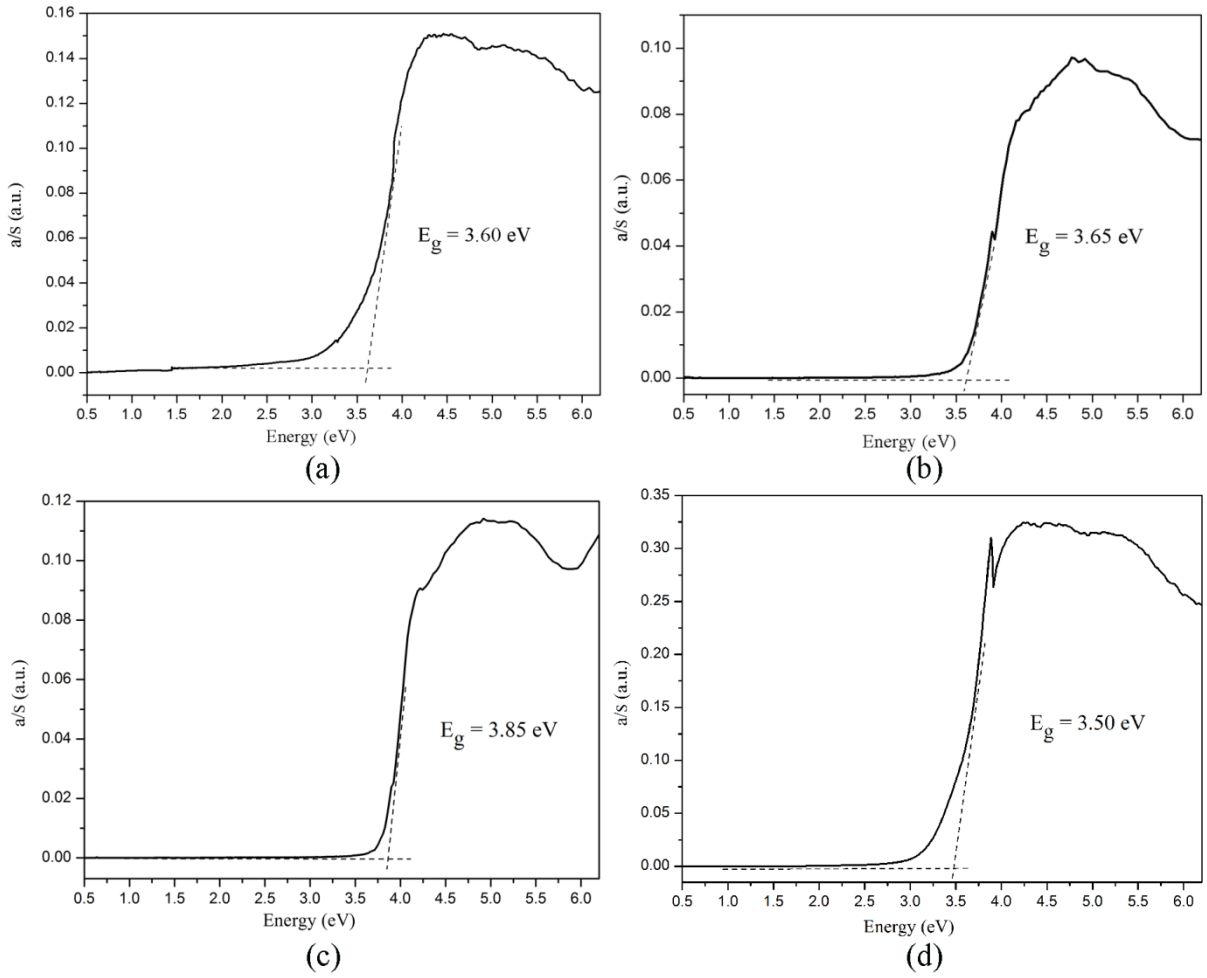

Fig. S5 UV−Vis diffuse reflectance spectra of **1** (a), **2** (b), **3** (c) and **4** (d).

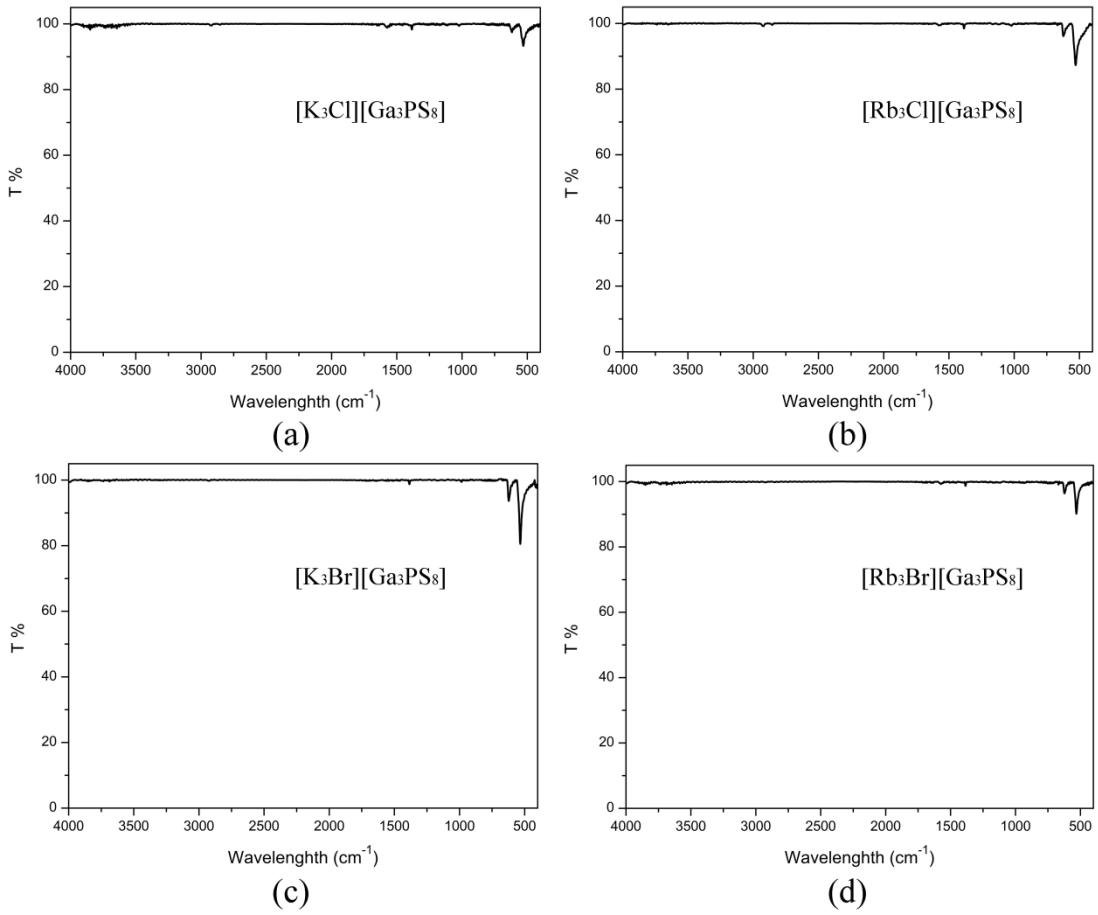

Fig. S6 IR spectra of **1** (a), **2** (b), **3** (c) and **4** (d).

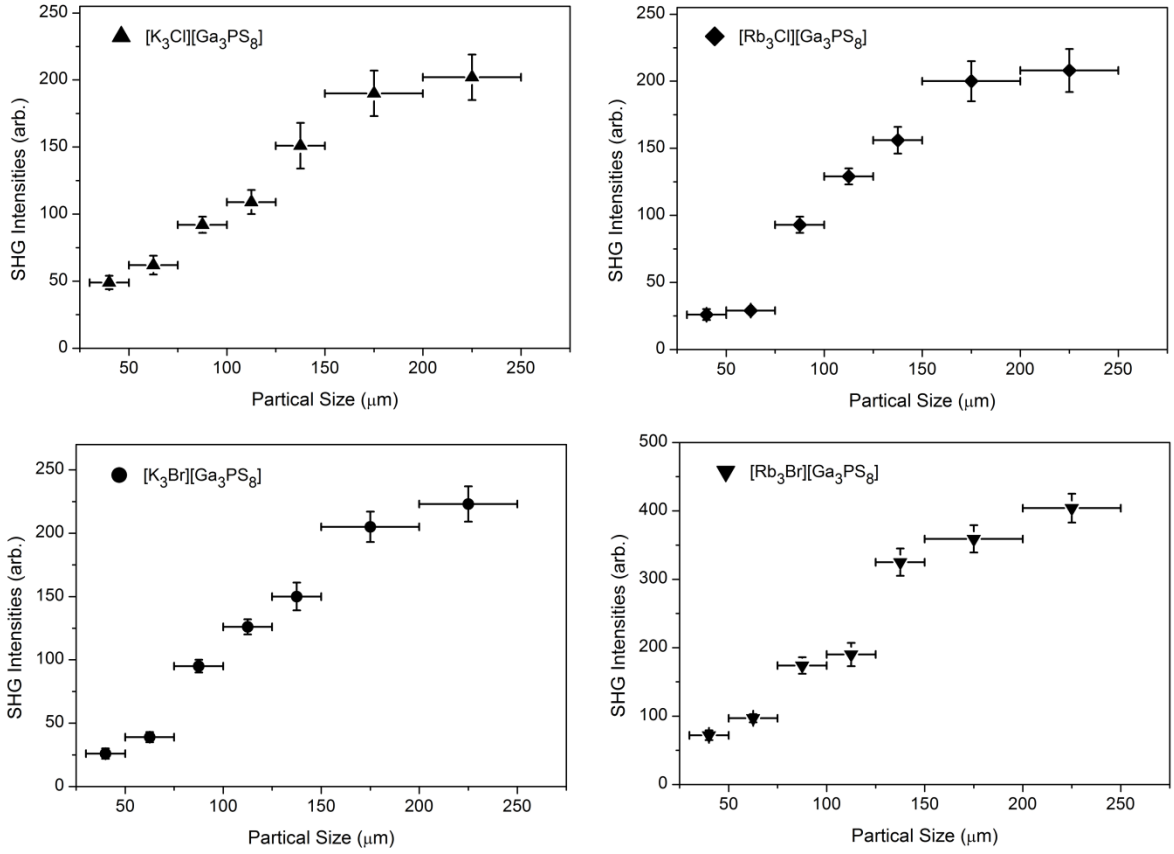

Fig. S7 Phase-matching results of **1**-**4** with the incident laser of 1950 nm. The particle size deviation and the SHG intensity deviation depending on the rotation angle are respectively indicated by horizontal and vertical error bars.

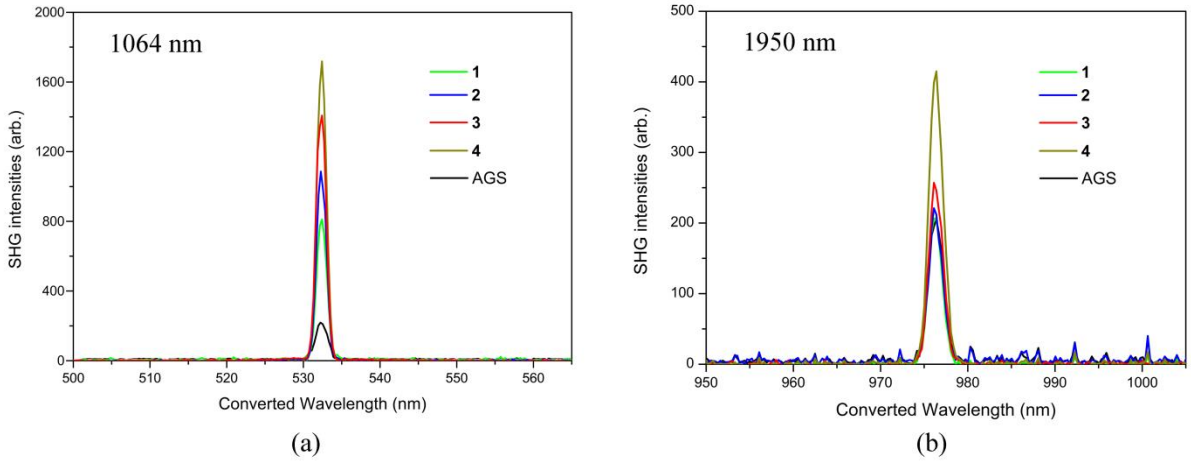

Fig. S8 SHG signals of **1**-**4** and AGS (reference) at the incident laser of 1064 nm (a) and 1950 nm (b) in the same particle size (200-250 μm).

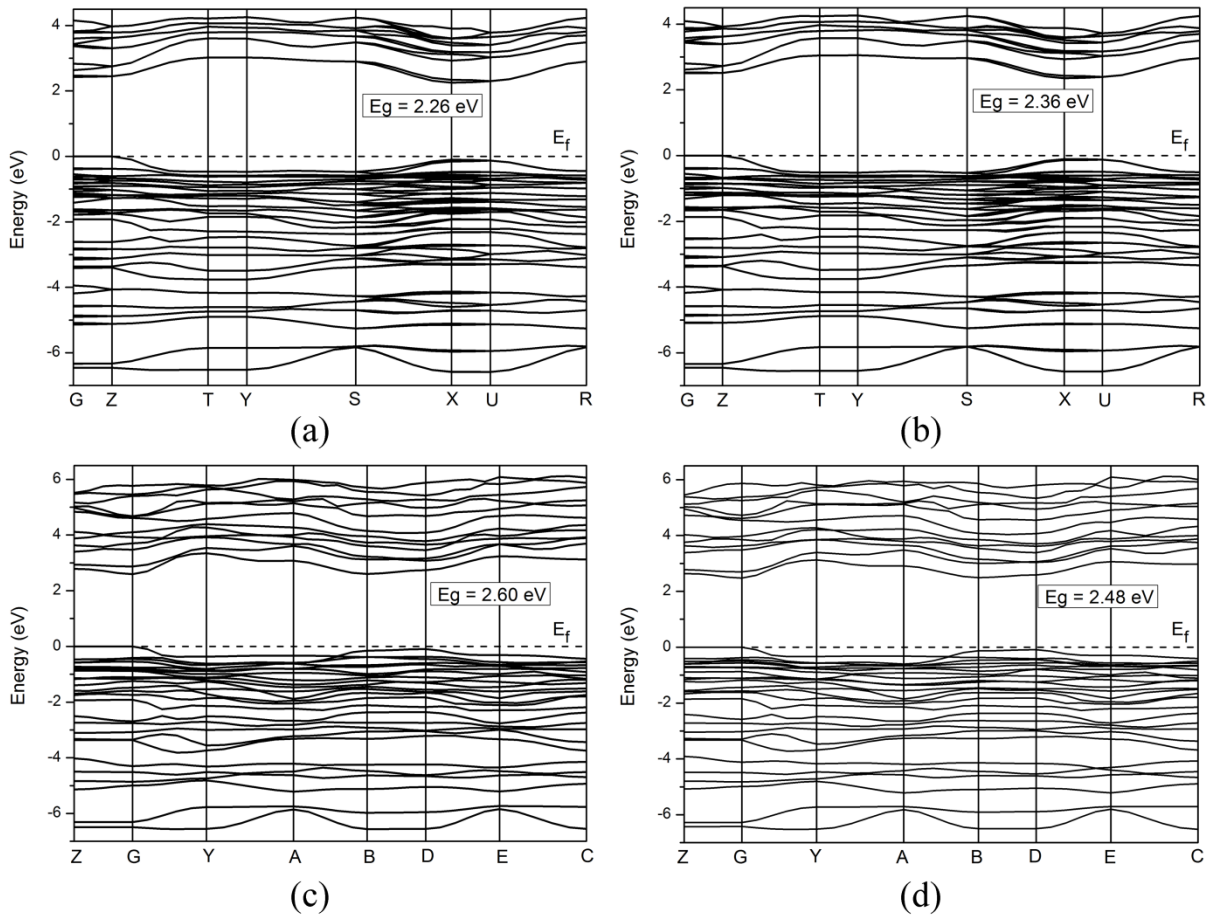

Fig. S9 Band structures of **1** (a), **2** (b), **3** (c) and **4** (d). The Fermi level is set at 0 eV for all the band structures.

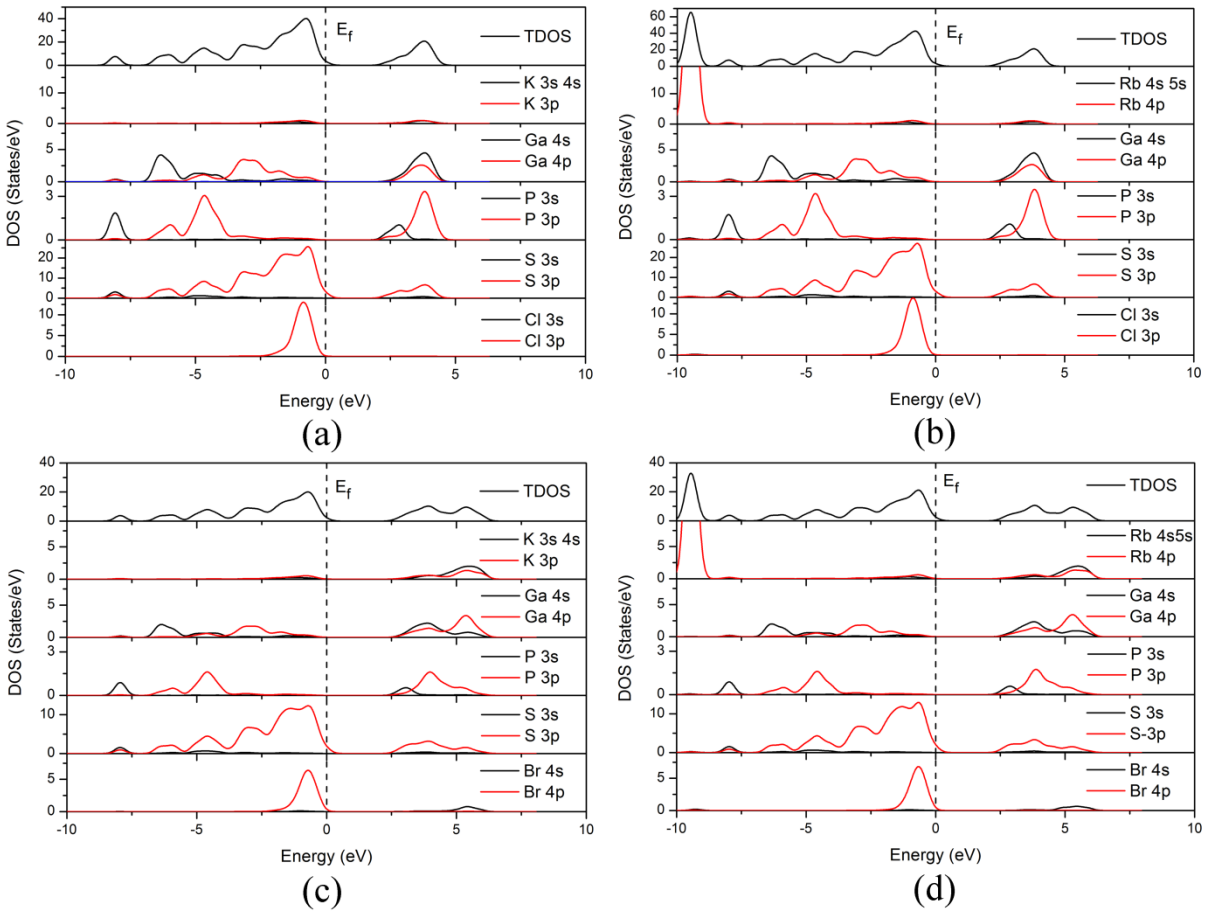

Fig. S10 Total and partial density of states (DOS) of **1** (a), **2** (b), **3** (c) and **4** (d).

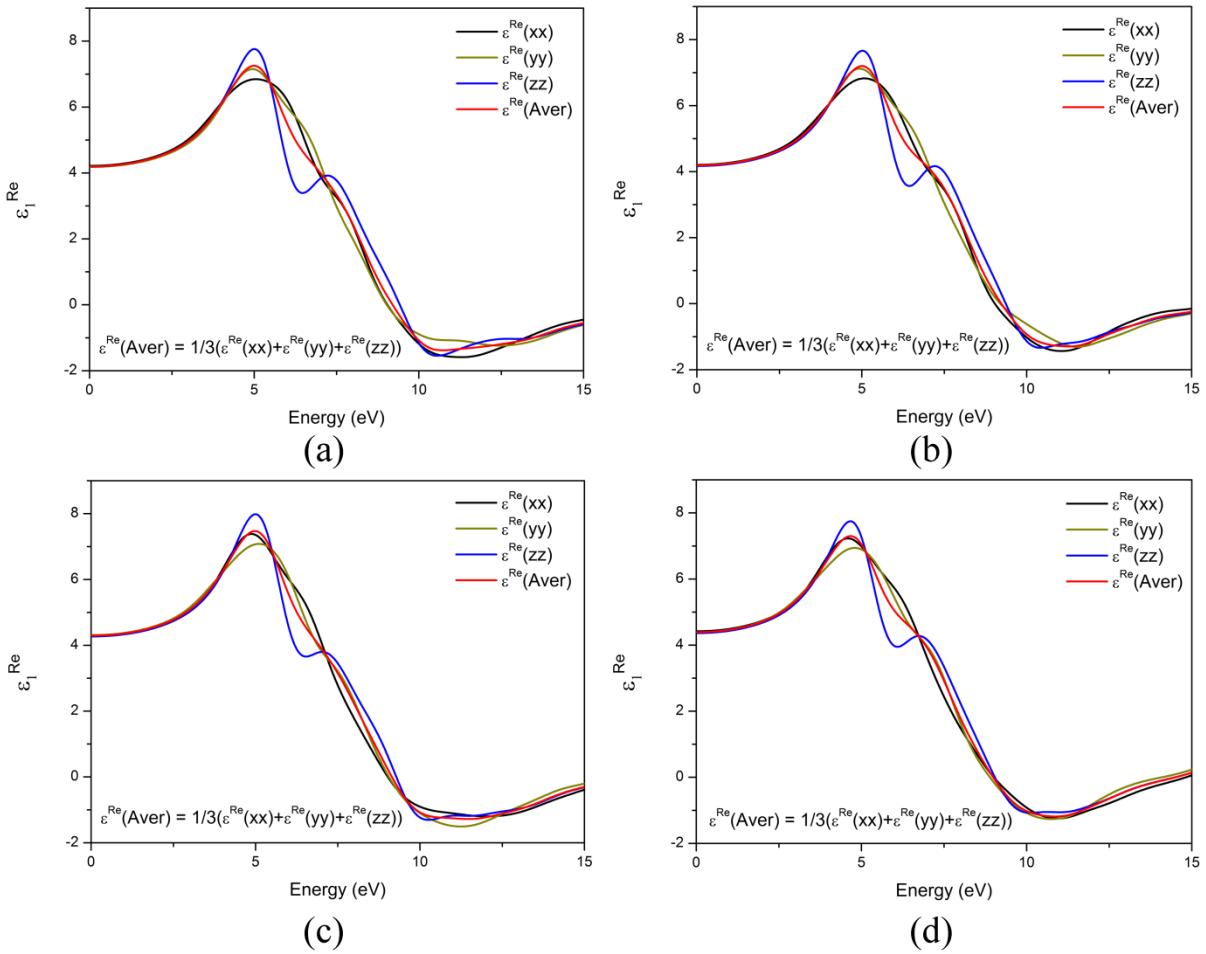

Fig. S11 Calculated real part ε_1 of dielectric functions of **1** (a), **2** (b), **3** (c) and **4** (d).

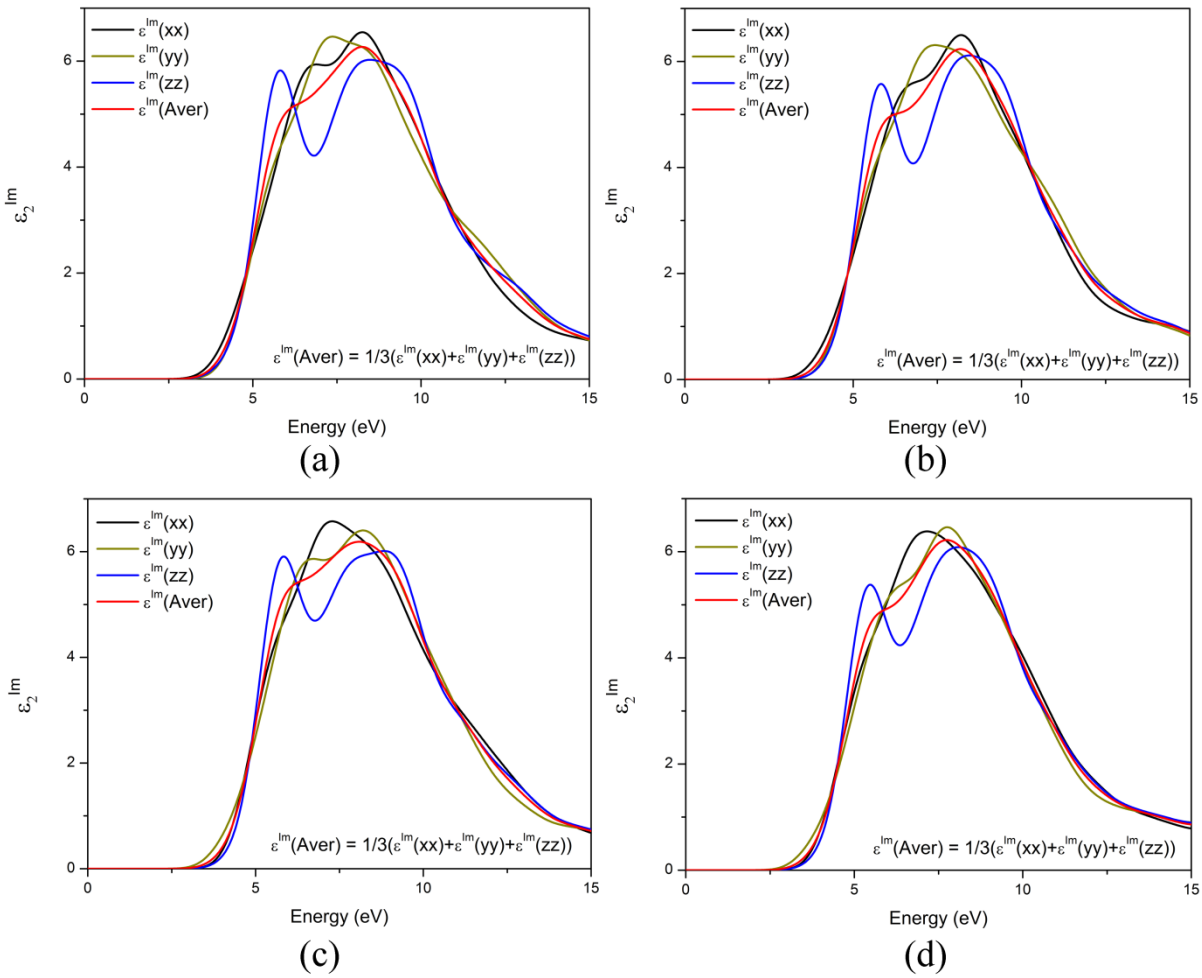

Fig. S12 Calculated imaginary part ε_2 of dielectric functions of **1** (a), **2** (b), **3** (c) and **4** (d).

Table S1. Crystal Data and Structure Refinements for **1**-**4**.

formula	$[K_3Cl][Ga_3PS_8]$ (**1**)	$[Rb_3Cl][Ga_3PS_8]$ (**2**)	$[K_3Br][Ga_3PS_8]$ (**3**)	$[Rb_3Br][Ga_3PS_8]$ (**4**)
fw	649.36	788.47	693.82	832.93
crystal color	colorless	colorless	Colorless	colorless
space group	$Pmn2_1$	$Pmn2_1$	Pm	Pm
a (Å)	7.202(1)	7.199(2)	6.378(2)	6.466(2)
b (Å)	6.357(1)	6.413(1)	7.178(2)	7.210(2)
c (Å)	17.839(3)	18.370(4)	9.467(3)	9.752(3)
β ( )	90	90	107.131(4)	107.029(4)
V (Å^3)	816.7(3)	848.0(3)	414.2(2)	434.6(2)
Z	2	2	1	1
D_{calcd} (g cm^{-3})	2.641	3.088	2.782	3.182
μ (mm^{-1})	6.929	14.491	9.083	16.281
GOF on F^2	1.128	1.064	0. 962	0.978
$R_1{}^a$ ($I > 2\sigma(I)$)	0.0375	0.0303	0.0249	0.0323
$wR_2{}^b$ ($I > 2\sigma(I)$)	0.0936	0.0545	0.0395	0.0651
$R_1{}^a$ (all data)	0.0405	0.0316	0.0260	0.0344
$wR_2{}^b$ (all data)	0.0970	0.0552	0.0406	0.0666
flack x	0.00(2)	0.00(1)	0.00(1)	0.03(1)
$\Delta\rho_{max}/\Delta\rho_{min,}$ (e.Å^{-3})	1.561/−0.624	0.994/−0.611	0.536/−0.555	0.709/−0.779

$^aR = \Sigma||F_o|-|F_c||/\Sigma|F_o|$, $^bwR = (\Sigma(w(F_o{}^2-F_c{}^2)^2)/\Sigma(w(F_o{}^2)^2))^{1/2}$.

Table S2. Selected Interatomic Distances (Å) in **1**-**4**.

bond	bond lengths			
	1	**2**	**3**	**4**
Ga(1)-S(2)	2.234(2)	2.232(2)	2.228(1)	2.240(2)
Ga(1)-S(4)	2.237(2)	2.233(2)	2.227(1)	2.232(2)
Ga(1)-S(1)	2.310(2)	2.314(2)	2.324(2)	2.329(3)
Ga(1)-S(6)	2.316(2)	2.317(2)	2.323(1)	2.337(2)
Ga(2)-S(2)×2	2.234(2)	2.228(2)	2.225(1)	2.230(2)
Ga(2)-S(6)	2.328(3)	2.333(2)	2.337(2)	2.357(3)

Ga(2)-S(5)	2.331(3)	2.341(3)	2.325(2)	2.330(4)
P(1)-S(3)	2.044(4)	2.028(3)	1.994(3)	2.061(5)
P(1)-S(1)×2	2.086(2)	2.080(2)	2.072(2)	2.075(3)
P(1)-S(5)	2.112(4)	2.101(3)	2.080(2)	2.093(4)
X(1)-A(1)	3.155(5)	3.200(3)	3.258(2)	3.308(2)
X(1)-A(1)	3.285(6)	3.282(3)	3.277(2)	3.310(2)
X(1)-A(2)×2	3.690(1)	3.675(1)	3.644(1)	3.653(1)
X(1)-A(3)	2.972(5)	3.094(3)	3.123(2)	3.247(2)

X=Cl, A= K for **1**; X=Cl, A= Rb for **2**; X=Br, A= K for **3**; X=Br, A= Rb for **4**.

Table S3. Selected Bond Angles (deg) in **1**-**4**.

bond	bond angle (deg)			
	1	**2**	**3**	**4**
S(2)-Ga(1)-S(4)	113.84(9)	112.86(8)	116.21(6)	115.08(10)
S(2)-Ga(1)-S(1)	112.84(9)	112.88(7)	112.02(6)	111.94(10)
S(4)-Ga(1)-S(1)	105.93(10)	106.51(8)	103.71(7)	104.62(11)
S(2)-Ga(1)-S(6)	109.15(9)	110.71(8)	109.85(6)	111.07(10)
S(4)-Ga(1)-S(6)	105.02(8)	104.86(8)	105.13(6)	104.81(9)
S(1)-Ga(1)-S(6)	109.70(9)	108.58(8)	109.49(6)	108.83(10)
S(2)-Ga(2)-S(2)	112.92(12)	113.05(10)	112.64(8)	112.10(13)
S(2)-Ga(2)-S(6)	106.82(7)	107.32(6)	106.38(4)	106.63(8)
S(2)-Ga(2)-S(6)	106.82(7)	107.32(6)	106.38(4)	106.63(8)
S(2)-Ga(2)-S(5)	112.28(7)	111.79(6)	112.80(5)	112.63(9)
S(2)-Ga(2)-S(5)	112.28(7)	111.79(6)	112.80(5)	112.63(9)
S(6)-Ga(2)-S(5)	105.09(10)	105.03(10)	105.11(7)	105.62(13)
S(3)-P(1)-S(1)	105.70(11)	106.05(9)	107.23(7)	106.61(13)
S(3)-P(1)-S(1)	105.70(11)	106.05(9)	107.23(7)	106.61(13)
S(1)-P(1)-S(1)	114.66(16)	113.70(13)	111.88(12)	112.47(18)
S(3)-P(1)-S(5)	107.86(16)	107.90(14)	107.97(12)	107.0(2)
S(1)-P(1)-S(5)	111.19(10)	111.34(9)	111.15(7)	111.85(13)
S(1)-P(1)-S(5)	111.19(10)	111.34(9)	111.15(7)	111.85(13)
A(3)-X(1)-A(1)	113.77(15)	112.65(9)	119.25(5)	118.32(6)
A(3)-X(1)-A(1)	84.66(13)	84.13(8)	85.92(6)	86.32(5)
A(1)-X(1)-A(1)	161.57(18)	163.22(10)	154.83(7)	155.36(8)
A(3)-X(1)-A(2)	102.07(7)	101.15(5)	98.87(3)	98.42(3)
A(1)-X(1)-A(2)	81.96(8)	82.80(5)	95.11(3)	82.55(3)
A(1)-X(1)-A(2)	94.58(8)	94.28(5)	81.74(3)	94.46(3)
A(3)-X(1)-A(2)	102.07(7)	101.15(5)	98.87(3)	98.42(3)
A(1)-X(1)-A(2)	81.96(8)	82.80(5)	95.11(3)	82.55(3)

A(1)-X(1)-A(2)	94.58(8)	94.28(5)	81.74(3)	94.46(3)
A(2)-X(1)-A(2)	154.85(15)	156.79(10)	160.08(7)	161.40(6)

X=Cl, A= K for **1**; X=Cl, A= Rb for **2**; X=Br, A= K for **3**; X=Br, A= Rb for **4**.

Table S4. Quantitative inductively coupled plasma (ICP) emission spectra results showing the mass percentages of element in **1**-**4**.

%	A	Ga	P	S	X
1 (Cal)	18.1	32.2	4.8	\	\
2 (Cal)	\	26.5	3.9	\	\
3 (Cal)	16.9	30.1	4.5	\	\
4 (Cal)	\	25.1	3.7	\	\
1 (Exp)	16.6	31.7	4.4	\	\
2 (Exp)	\	27.1	3.9	\	\
3 (Exp)	15.6	29.9	4.7	\	\
4 (Exp)	\	26.2	3.5	\	\

Table S5. Powder Laser Induced Damage Thresholds (LIDTs).

compounds	laser energy (mJ)	spot diameter (mm)	damage threshold [MW cm^{-2}]
1	48.3	2.8	78.5
2	46.0	2.8	74.7
3	39.7	2.8	64.5
4	37.7	2.8	61.2
AGS	1.2	2.8	2.0

3. References

1 Rigaku, *CrystalClear, version 1.3.5*; Rigaku Corporation: Tokyo, 2002.

2 Siemens, *SHELXTL Version 5 Reference Manual*; Siemens Energy &Automation Inc.: Madison, WI, 1994.

3 A. L. Spek, *PLATON, A Multipurpose Crystallographic Tool*; Utrecht University, Utrecht, The Netherlands, 2005.

4 L. M. Gelato and E. Parthé , *J. Appl. Crystallogr*, 1987, **20**, 139−143.

5 G. Korum, *Reflectance Spectroscopy*, Springer, New York, 1969.

6 M. D. Segall, P. L. D. Lindan, M. J. Probert, C. J. Pickard, P. J. Hasnip, S. J. Clark and M. C. Payne, *J. Phys.: Condens. Matter*, 2002, **14**, 2717−2744.

7 J. P. Perdew, K. Burke and M. Ernzerhof, *Phys. Rev. Lett*. 1996, **77**, 3865−3868.

8 (a) D. R. Hamann, M. Schluter and C. Chiang, *Phys. Rev. Lett.* 1979, **43**, 1494−1497. (b) J. S. Lin, A. Qteish, M. C. Payne, V. Heine, *Phys. Rev. B* 1993, **47**, 4174−4180.

9 C. M. I. Okoye, *J. Phys. Condens. Matter,* 2003, **15**, 5945−5958.

10 (a) S. Laksari, A. Chahed, N. Abbouni, O. Benhelal and B. Abbar, *Comput. Mater. Sci.* 2006, **38**, 223−230. (b) S. D. Mo and W. Y. Ching, *Phys. Rev. B* 1995, **51**, 13023−13032.

11 R. W. Boyd, *Nonlinear Optics*, Academic Press: New York, 1992; pp 21−32.